

MLICv2: Enhanced Multi-Reference Entropy Modeling for Learned Image Compression

Wei Jiang¹ Yongqi Zhai¹ Jiayu Yang² Feng Gao³ Ronggang Wang^{1,2}

Abstract

Recent advances in learned image compression (LIC) have achieved remarkable performance improvements over traditional codecs. Notably, the MLIC series—LICs equipped with multi-reference entropy models—have substantially surpassed conventional image codecs such as Versatile Video Coding (VVC) Intra. However, existing MLIC variants suffer from several limitations: performance degradation at high bitrates due to insufficient transform capacity, suboptimal entropy modeling that fails to capture global correlations in initial slices, and lack of adaptive channel importance modeling. In this paper, we propose MLICv2 and MLICv2⁺, enhanced successors that systematically address these limitations through improved transform design, advanced entropy modeling, and exploration of the potential of instance-specific optimization. For transform enhancement, we introduce a lightweight token mixing block inspired by the MetaFormer architecture, which effectively mitigates high-bitrate performance degradation while maintaining computational efficiency. For entropy modeling improvements, we propose hyperprior-guided global correlation prediction to extract global context even in the initial slice of latent representation, complemented by a channel reweighting module that dynamically emphasizes informative channels. We further explore enhanced positional embedding and guided selective compression strategies for superior context modeling. Additionally, we apply the Stochastic Gumbel Annealing (SGA) to demonstrate the potential for further performance improvements through input-specific optimization. Extensive experiments demonstrate that MLICv2 and MLICv2⁺ achieve state-of-the-art results, reducing Bjøntegaard-Delta Rate by 16.54%, 21.61%, 16.05% and 20.46%, 24.35%, 19.14% on Kodak, Tecnick, and CLIC Pro Val datasets, respectively, compared to VTM-17.0 Intra.

1. Introduction

Image compression constitutes a fundamental challenge in multimedia communication, with the objective of achieving compact representation while preserving reconstruction quality. Traditional compression methods, exemplified by VVC Intra [12], rely on block-based hybrid coding frameworks refined over decades. However, as conventional approaches near performance saturation, learned image compression (LIC) has emerged as a transformative paradigm, demonstrating substantial potential to surpass hand-crafted codecs through end-to-end optimization.

Contemporary LIC methods [9, 10, 15, 16, 19, 26, 30, 31, 32, 33, 34, 35, 38, 45, 50, 51, 53, 64, 68, 71, 74, 75, 78, 86, 87, 88] predominantly adopt autoencoder-based frameworks with rate-distortion optimization, comprising analysis transforms, quantization, synthesis transforms, and entropy models. The analysis transform maps input images to latent representations, which undergo quantization before reconstruction via synthesis transforms. Entropy models estimate quantized latent distributions to facilitate efficient entropy coding. Advanced techniques of transform architectures and entropy models have enabled several LICs [20, 30, 32, 33, 34, 40, 45, 47] to achieve performance comparable to or exceeding advanced traditional codecs like VVC Intra [12].

¹Guangdong Provincial Key Laboratory of Ultra High Definition Immersive Media Technology, Shenzhen Graduate School, Peking University ²Pengcheng Laboratory ³School of Arts, Peking University. Correspondence to: Wei Jiang <wei.jiang1999@outlook.com>, Ronggang Wang <rgwang@pku.edu.cn>.

Entropy modeling plays a pivotal role in LIC performance, aiming to minimize conditional entropy through informative prior capture. While hyperprior models [10] provide side information, context models [31, 52] capture spatial dependencies between previously decoded and current elements. Building on these foundations, Jiang *et al.* introduced the MLIC series [33, 34], which leverages multi-reference priors through latent representation partitioning into channel-wise slices [51], capturing both inter-slice and intra-slice dependencies. MLIC employs checkerboard partitioning [31] within slices for two-pass decoding, while attention mechanisms model global dependencies from previous slices. MLIC⁺⁺ [33] addressed computational complexity by replacing vanilla attention [70] with linear attention [60] and modeling global correlations across previous slices.

Despite the strong overall performance of the MLIC series, several critical limitations persist and motivate our work. First, regarding transform design, MLIC models exhibit performance degradation at high bitrates, primarily attributed to insufficient transform capacity for preserving latent representation information. Second, concerning entropy modeling, global correlation estimation relies exclusively on previous slices, precluding global correlation capture in initial slices. Moreover, existing approaches treat all channels equally without considering varying informational importance, potentially limiting entropy modeling accuracy.

To systematically address these limitations, we propose MLICv2, featuring enhanced transform and entropy modeling modules, and MLICv2⁺, which additionally incorporates iterative refinement techniques [80] to demonstrate framework potential.

For transform improvement, we design an efficient token mixing block replacing residual blocks in MLIC⁺⁺. Inspired by MetaFormer architecture [81], our block employs depth-wise convolution for spatial token mixing and lightweight gated interaction for point-wise operations, achieving superior high-bitrate performance with reduced complexity.

For entropy modeling enhancement, we propose MEMv2, an advanced multi-reference entropy model capturing diverse dependencies. We introduce hyperprior-guided global correlation prediction for initial slices, leveraging spatial distribution similarity between hyperprior and latent representations. Our two-stage context modeling strategy performs spatial aggregation followed by adaptive channel-wise reweighting to capture feature importance variations. Additional improvements include 2D Rotary Positional Embedding (RoPE) and guided selective compression for enhanced modeling and coding efficiency.

Additionally, we employ Stochastic Gumbel Annealing (SGA) [80] to iteratively refine latent representations and side information for each input. This approach demonstrates our framework’s potential for input-specific rate-distortion optimization while preserving decoder complexity, suggesting opportunities for further architectural enhancements.

Our comprehensive approach yields significant improvements, with MLICv2 and MLICv2⁺ substantially outperforming MLIC⁺⁺ as demonstrated in Figure 1. MLICv2 achieves BD-rate reductions of 16.54%, 21.61%, and 16.05% on Kodak, Tecnick, and CLIC Pro Val datasets respectively, while MLICv2⁺ further improves these results to 20.46%, 24.35%, and 19.14% over VTM-17.0 Intra. Our contributions are summarized as follows:

- We introduce MetaFormer-based architecture for LIC through our simple token mixing block, achieving superior high-bitrate performance with reduced computational complexity compared to previous residual blocks.
- We systematically improve entropy modeling through multiple improvements: (i) hyperprior-guided global correlation prediction addressing initial slice limitations, (ii) the first two-stage context modeling strategy with spatial aggregation and adaptive channel reweighting, and (iii) advanced positional embedding and selective compression mechanisms.
- We demonstrate the effectiveness of our framework by applying iterative refinement techniques (SGA), showing consistent performance gains without decoder complexity increase and suggesting opportunities for further architectural

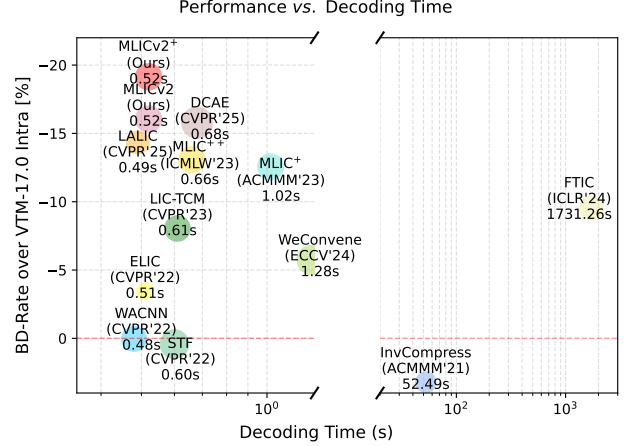


Figure 1: BD-Rate and decoding time during inference on CLIC Professional Valid [65] with 2K resolution. The bubble size indicates the number of model parameters.

enhancements.

- Extensive experiments validate our approach, with MLICv2 and MLICv2⁺ achieving BD-rate reductions of 16.54%, 21.61%, 16.05% and 20.46%, 24.35%, 19.14% over VTM-17.0 Intra on Kodak, Tecnick, and CLIC Pro Val datasets respectively.

2. Related Works

2.1. Learned Image Compression

Autoencoder-based learned image compression [9, 16, 30, 32, 33, 34, 50, 51, 64] follows the transform coding paradigm, consisting of an analysis transform g_a with parameters ϕ , a synthesis transform g_s with parameters ψ , a quantization function $\lceil \cdot \rceil$, and an entropy model p with parameters ρ . Given an input image $\mathbf{x} \sim p_{\mathbf{x}}$, the process is formulated as:

$$\mathbf{y} = g_a(\mathbf{x}; \phi), \hat{\mathbf{y}} = \lceil \mathbf{y} \rceil, \hat{\mathbf{x}} = g_s(\hat{\mathbf{y}}; \psi). \quad (1)$$

The rate-distortion optimization is achieved through:

$$\mathcal{L} = \mathbb{E}_{\mathbf{x} \sim p_{\mathbf{x}}} \left[\underbrace{-\log_2 \int p(\hat{\mathbf{y}}; \rho) d\hat{\mathbf{y}}}_{\text{bit-rate}} + \lambda \times \underbrace{\mathcal{D}(\hat{\mathbf{x}}, \mathbf{x})}_{\text{distortion}} \right], \quad (2)$$

where λ balances the rate-distortion trade-off. During training, quantization is approximated by adding uniform noise [9] or straight-through estimation [64]. Ballé *et al.* [10] introduce hyperprior networks using hyper analysis h_a and hyper synthesis h_s to improve entropy estimation through quantized side information $\hat{\mathbf{z}}$ extracted from latent representations.

Transform architectures have evolved significantly, incorporating Generalized Divisive Normalization (GDN) [8], residual non-local attention [15, 85], deep residual networks [16], and transformer-based designs [48, 87, 88]. Mixed CNN-transformer [45] and Mamba [25, 56, 82] architectures have also been explored for capturing both local and non-local interactions. Entropy estimation has progressed from simple univariate Gaussian models [10] to sophisticated approaches including mean-scale Gaussian models [50], asymmetric Gaussian distributions [17], Gaussian mixture models [16], and generalized Gaussian models [83], significantly improving compression efficiency.

2.2. Conditional Entropy Models

Conditional entropy models leverage context $\hat{\mathbf{C}}$ to reduce bit-rate, exploiting the principle that conditional entropy is bounded by unconditional entropy:

$$\mathcal{H}(\hat{\mathbf{y}}|\hat{\mathbf{C}}) \leq \mathcal{H}(\hat{\mathbf{y}}). \quad (3)$$

Local context has evolved from serial approaches like PixelCNN [50, 69] to efficient parallel methods including zigzag scanning [41] and checkerboard partitioning [30]. These intra-slice local contexts are complemented by inter-slice approaches and channel-wise autoregressive coding [51] for faster decoding.

Recent works investigate long-range correlations among distant elements [26, 33, 34, 36, 55]. Qian *et al.* [54, 55] employ neighbor elements and bi-directional attention for global correlation estimation. Guo *et al.* [26] utilize L-2 distance metrics, while Kim *et al.* [36] transmit global information to decoders. Recently, Jiang *et al.* [34] propose MLIC and MLIC⁺, dividing global contexts into inter-slice and intra-slice components. The latent representation is partitioned into multiple slices for autoregressive conditional coding, employing checkerboard attention for intra-slice contexts and convolutional layers for inter-slice contexts. However, the quadratic complexity of vanilla attention [70] limits scalability for high-resolution images, which is addressed by MLIC⁺⁺ [33] through linear attention mechanisms [60].

3. Method

3.1. Background: MLIC⁺⁺

Our proposed MLICv2 and MLICv2⁺ build upon the foundation established by MLIC⁺⁺ [33]. MLIC⁺⁺ employs a simplified version of Cheng’20’s transform [16], where attention modules are removed to reduce computational complexity.

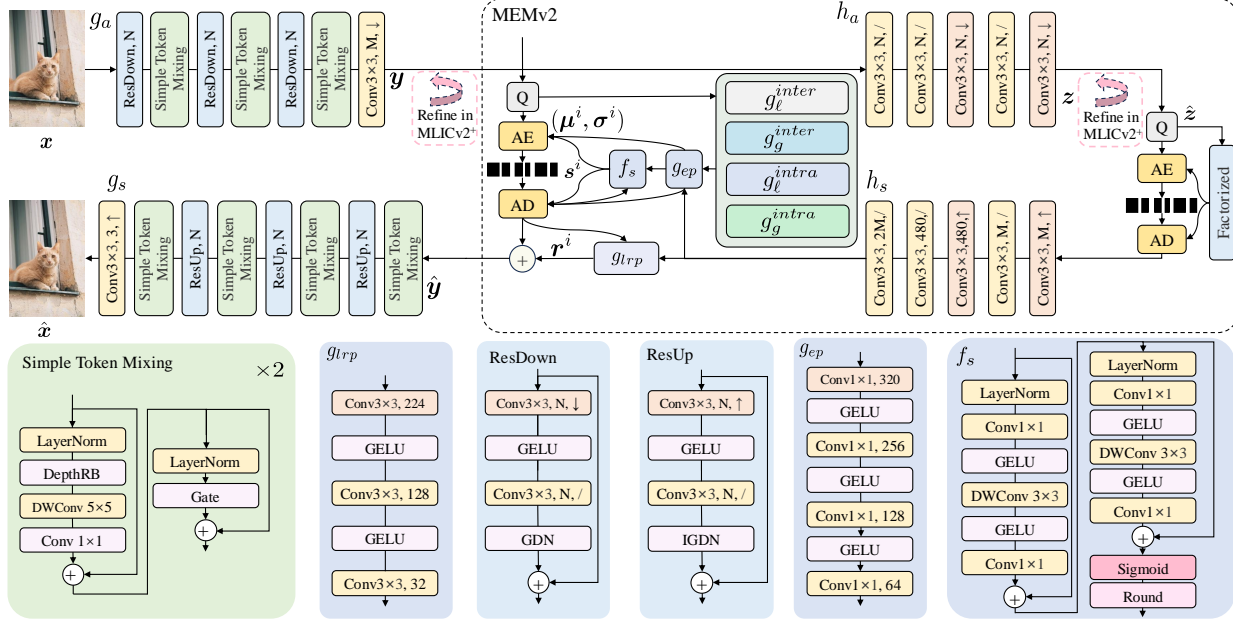


Figure 2: The overall architecture of MLICv2/MLICv2⁺. g_a is the analysis transform, g_s is the synthesis transform, h_a is the hyper analysis, and h_s is the hyper synthesis. g_{ep} is the entropy parameter module. f_s is the selective compression predictive module. g_{lrp} is the latent residual prediction module [51]. AE and AD are arithmetic encoding and decoding. \uparrow denotes upsampling and \downarrow denotes downsampling. x is the input image and \hat{x} is the reconstructed image. y is the latent representation and \hat{y} is the quantized latent representation. \hat{y}^i is the i -th slice of \hat{y} . μ^i, σ^i are the mean and scale of \hat{y}^i . s^i is the predicted selective coding map. r^i is the predicted residual. \hat{z} is the side information. M, N are the channel numbers, which are 320, 192 in MLICv2/MLICv2⁺. “Refine” is employed in MLICv2⁺.

For entropy modeling, MLIC⁺⁺ introduces a linear-complexity multi-reference entropy model (MEM⁺⁺), which effectively captures hyperprior, intra-slice, and inter-slice dependencies.

The hyperprior information \hat{H} is derived from side information \hat{z} . Following the approach of Minnen *et al.* [51], the latent representation \hat{y} is partitioned into $L + 1$ slices: $\hat{y}^0, \hat{y}^1, \dots, \hat{y}^L$. Each slice \hat{y}^i is further divided into anchor \hat{y}_{ac}^i and non-anchor \hat{y}_{na}^i components using checkerboard partitioning [31].

The inter-slice local context module g_{ℓ}^{inter} captures inter-slice local context $\hat{C}_{\ell}^{<i}$ from preceding slices $\hat{y}^{<i}$. To model inter-slice global context $\hat{C}_g^{<i}$, MLIC⁺⁺ employs linear attention [60] to achieve an optimal balance between performance and computational complexity. The intra-slice local context \hat{C}_{ℓ}^i is extracted from the anchor partition \hat{y}_{ac}^i using overlapped window-based checkerboard attention g_{ℓ}^{intra} .

A key insight in MLIC⁺⁺ is that feature maps from different slices exhibit similar global similarity patterns, as they can be viewed as thumbnails of the same content. Therefore, the attention maps between anchor and non-anchor parts of the $(i - 1)$ -th slice are leveraged to predict global similarities for the current slice. The intra-slice global context \hat{C}_g^i is extracted from \hat{y}_{ac}^i via the predicted attention map and the intra-slice global context module g_g^{intra} . This process is formulated as:

$$\begin{aligned} \hat{C}_{\ell}^{<i} &= g_{\ell}^{inter}(\hat{y}^{<i}), \hat{C}_g^{<i} = g_g^{inter}(\hat{y}^{<i}), \\ \hat{C}_{\ell}^i &= g_{\ell}^{intra}(\hat{y}_{ac}^i), \hat{C}_g^i = g_g^{intra}(\hat{y}_{ac}^{i-1}, \hat{y}_{na}^{i-1}, \hat{y}_{ac}^i). \end{aligned} \quad (4)$$

The estimated means μ_{ac}^i, μ_{na}^i and scales $\sigma_{ac}^i, \sigma_{na}^i$ are extracted from the contextual information using the entropy parameter module g_{ep} . MLIC⁺⁺ incorporates mixed quantization [51] and the latent residual prediction module g_{lrp} [51]. In mixed quantization, zero-centered straight-through estimation (STE) [64] is applied for distortion computation, while additive uniform noise (AUN) [9] is used for entropy estimation during training. The module g_{lrp} predicts quantization

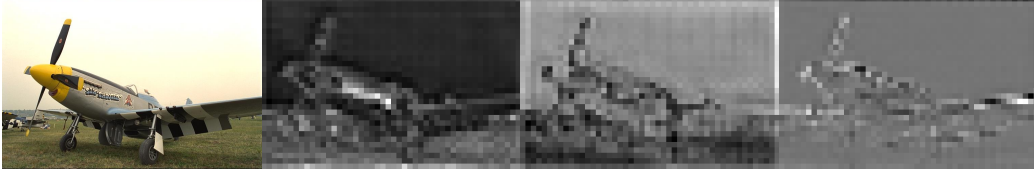


Figure 3: Visualization of the channels of hyperprior \hat{H} ($\lambda = 0.013$). \hat{H} extracted from the latent representation of Image Kodim20 exhibits similar global similarity to original Kodim20.

residuals based on decoded slices and hyperprior information:

$$\begin{aligned}\hat{y}_{ac}^i &= \text{STE}(\mathbf{y}_{ac}^i - \boldsymbol{\mu}_{ac}^i) + \boldsymbol{\mu}_{ac}^i + \mathbf{r}_{ac}^i, \\ \hat{y}_{na}^i &= \text{STE}(\mathbf{y}_{na}^i - \boldsymbol{\mu}_{na}^i) + \boldsymbol{\mu}_{na}^i + \mathbf{r}_{na}^i,\end{aligned}\quad (5)$$

where

$$\mathbf{r}_{ac}^i = g_{lrp}(\hat{\mathbf{y}}^{<i}, \hat{H}), \mathbf{r}_{na}^i = g_{lrp}(\hat{\mathbf{y}}^{<i}, \hat{y}_{ac}^i, \hat{H}). \quad (6)$$

3.2. Overall Architecture

Figure 2 illustrates the overall architecture of our proposed MLICv2 and MLICv2⁺. MLICv2 preserves the fundamental structure of MLIC⁺⁺ while introducing several key enhancements to improve compression efficiency, particularly at high bit rates. First, we replace residual blocks following downsampling and upsampling operations with lightweight token mixing blocks, which enhance representational capacity while reducing computational complexity. Second, we upgrade the multi-reference entropy model to MEMv2 by incorporating enhanced inter-slice and intra-slice context modules with context reweighting and advanced positional embedding to better capture latent dependencies. Third, we introduce a selective compression module f_s that intelligently predicts and skips zero elements in latent representations, reducing both bit rate and arithmetic coding time without compromising reconstruction quality. To demonstrate the potential for input-specific optimization, we propose MLICv2⁺, which iteratively refines latent features \mathbf{y} and side information \mathbf{z} based on the rate-distortion characteristics of individual inputs, enabling tailored compression strategies for different content types.

3.3. Efficient Simple Token Mixing Transform

As illustrated in Figure 6, MLIC⁺⁺ exhibits performance degradation at high bit rates due to limited capacity of transform modules to retain sufficient information in latent representations [76]. The representational capacity is fundamentally influenced by the number of channels. As demonstrated by Ballé *et al.* [6], when channel numbers are limited, the performance gap between low- and high-capacity models is negligible at low bit rates. However, this gap becomes pronounced as bit rates increase, with higher-capacity models achieving significantly better reconstruction quality.

Simply increasing channel numbers often results in prohibitive computational complexity. A more practical approach is to enhance the architectural design itself to improve transform capacity without substantially increasing computational cost. Recent work has adopted transformer layers [46] for transform coding [40, 45, 48, 88], demonstrating remarkable performance improvements. However, existing techniques [45] can introduce up to twice the complexity of original residual blocks in the MLIC series.

Inspired by the elegance of MetaFormer [81], which consists of token mixing and channel-wise interaction components, we investigate its effectiveness for LIC. However, MetaFormer’s use of pooling for token mixing, while efficient, is suboptimal for compression tasks due to information loss. We propose a simple token mixing block as illustrated in Figure 2. For token mixing, we employ a depth-wise residual block (DepthRB) [32] for nonlinear embedding, depth-wise convolution for spatial token mixing, and a gate block [32] for efficient channel-wise interactions. LayerNorm (LN) [5] is adopted for stable training. Given input feature ω , the process is formulated as:

$$\begin{aligned}\omega &= \omega + \text{Conv1} \times 1(\text{DWConv5} \times 5(\text{DepthRB}(\text{LN}(\omega)))), \\ \omega &= \omega + \text{Gate}(\text{LN}(\omega)),\end{aligned}\quad (7)$$

where $\omega \in \mathbb{R}^{c \times h \times w}$ represents the input feature with c, h, w denoting channels, height, and width respectively. Stacking two

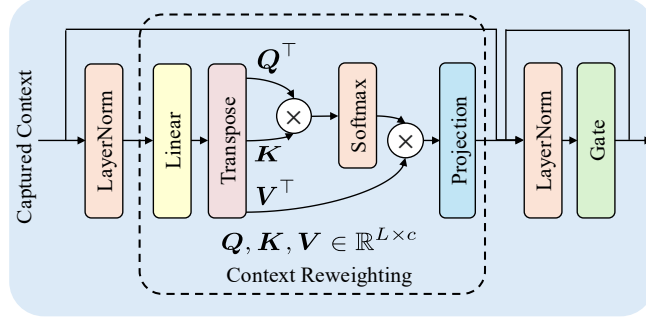


Figure 4: Proposed context reweighting module.

token mixing blocks creates deeper transforms with enhanced expressiveness. Compared to previous residual blocks [16] consisting of two 3×3 convolutions, our token mixing block achieves lower complexity while delivering significantly better performance, especially at high bit rates. The complexity analysis reveals that stacking *two* simple token-mixing blocks reduces multiply-accumulate operations (MACs) by 7.38% at $c = 192$ and by 8.87% at $c = 320$, compared with stacking a *single* residual block [16, 33, 34].

3.4. Enhanced Multi-Reference Entropy Modeling

The enhanced multi-reference entropy model (MEMv2) is presented in Figure 2. To address the limitations of MLIC⁺⁺, we introduce several key innovations: hyperprior-based global correlation prediction, context reweighting to handle varying channel importance, 2D Rotary Positional Embedding (RoPE) and guided selective compression for improved context modeling and entropy coding.

3.4.1. HYPERPRIOR-GUIDED GLOBAL CORRELATION PREDICTION

In MLIC⁺⁺ [33], global similarity between anchor and non-anchor parts of the previous slice is exploited to predict current slice similarities. However, for the first slice $\hat{\mathbf{y}}^0$, no such reference exists. The only available conditional information is the hyperprior $\hat{\mathbf{H}}$, obtained by upsampling side information $\hat{\mathbf{z}}$ extracted from latent representation \mathbf{y} . As illustrated in Figure 3, the hyperprior preserves global similarity patterns similar to the original image. We leverage this property by estimating global similarity between $\hat{\mathbf{y}}_{ac}^0$ and $\hat{\mathbf{y}}_{na}^0$ using the similarity between anchor and non-anchor parts of the hyperprior, $\hat{\mathbf{H}}_{ac}$ and $\hat{\mathbf{H}}_{na}$. Following MLIC⁺⁺, we employ linear attention [60] for global context modeling and introduce a Gate block [32] for enhanced pointwise interaction:

$$\begin{aligned}\hat{\mathbf{C}}_g^0 &= \text{Softmax}_2(\hat{\mathbf{H}}_{na,q}) \left(\text{Softmax}_1(\hat{\mathbf{H}}_{ac,k})^\top \hat{\mathbf{y}}_{g,v}^0 \right), \\ \hat{\mathbf{C}}_g^0 &= \text{Gate}(\hat{\mathbf{C}}_g^0) + \hat{\mathbf{C}}_g^0,\end{aligned}\tag{8}$$

where $\hat{\mathbf{H}}_{na,q} = \text{Linear}(\hat{\mathbf{H}}_{na})$, $\hat{\mathbf{H}}_{ac,k} = \text{Linear}(\hat{\mathbf{H}}_{ac})$, and $\hat{\mathbf{y}}_{g,v}^0 = \text{Linear}(\hat{\mathbf{y}}_{ac}^0)$.

While prior methods [30, 32, 33, 34] capture only local dependencies in the first slice, our hyperprior-guided mechanism models global dependencies effectively. Given the information compaction property of latent representations [30], the fact that the first slice typically exhibits higher entropy as it serves as reference for subsequent slices, incorporating global context significantly reduces bit rate and improves compression performance.

3.4.2. CONTEXT REWEIGHTING

In MLIC⁺⁺ [33], the contexts are extracted by spatial attention mechanism. Given the query $\mathbf{Q} \in \mathbb{R}^{L \times c}$, key $\mathbf{K} \in \mathbb{R}^{L \times c}$ and the value $\mathbf{V} \in \mathbb{R}^{L \times c}$, where $L = hw$ is the sequence length, h is the height, w is the width, and c is the channel number, in most spatial attention [60, 70], the attention map is computed by $\text{Sim}(\mathbf{Q}\mathbf{K}^\top) \in \mathbb{R}^{L \times L}$, where Sim is the predefined function, such as Softmax [70] or two independent Softmax operations [60], indicating the information is gathered and weighted from spatial tokens ($\in \mathbb{R}^{1 \times c}$). However, one common limitation is that all channel-wise features are treated equally, without considering that different channels may carry varying levels of importance. We argue that adaptively reweighting channel-wise context features can lead to more accurate entropy modeling. By suppressing noisy or less informative channels

and emphasizing more relevant ones, the model has the potential to capture context information more precisely and improve overall compression performance, which has not been considered in existing methods [19, 22, 30, 31, 33, 34, 51, 54, 55].

To address this issue, we introduce a two-stage context modeling strategy, where spatial aggregation [33] is first performed, followed by adaptive channel-wise context reweighting to capture the varying importance of different features. The architecture is in Fig. 4. Specifically, in context reweighting, the context is transformed to query Q , key K , and value V , and the query and values are transposed to compute the channel-wise attention map [3]. The process is formulated as:

$$O = \text{Softmax}(Q^\top K) V^\top.$$

The resolution of the attention map $\text{Softmax}(Q^\top K)$ is $c \times c$, indicating the importance of each channel ($\in \mathbb{R}^{L \times 1}$). The complexity of Eq. (8) is $\mathcal{O}(c^2 hw)$. O is then fed into a Gate block [32] for efficient point-wise interactions. This attention-based reweighting helps the model focus on the most relevant parts of the context. To the best of our knowledge, this is the first attempt to explicitly model channel-wise importance in context features for LIC. Our approach brings consistent performance improvements with minimal additional cost.

3.4.3. 2D ROTARY POSITION EMBEDDING

MLIC⁺⁺ [33] applies relative position embedding (RPE) from Swin-Transformer [46] directly to attention maps as additional bias. However, this direct addition may limit interaction with attention weights. Recently, Rotary Positional Embedding (RoPE) [63], a multiplication-based approach, has been widely adopted in language models [58, 66]. RoPE offers several advantages: compatibility with linear attention (whereas RPE requires adding biases that conflict with implicit attention computation), better extrapolation capabilities, and more concise implementation. For 2D image content, we extend the original 1D RoPE to handle horizontal, vertical, and diagonal relationships. Given query q_{m_x, m_y} and key k_{n_x, n_y} at 2D positions (m_x, m_y) and (n_x, n_y) , we rotate queries and keys twice with different angles θ_x and θ_y for horizontal and vertical directions. When $c = 2$, the rotation matrix for the query becomes:

$$\underbrace{\begin{bmatrix} \cos m_x \theta_x & -\sin m_x \theta_x \\ \sin m_x \theta_x & \cos m_x \theta_x \end{bmatrix}}_{\text{horizontal}} \underbrace{\begin{bmatrix} \cos m_y \theta_y & -\sin m_y \theta_y \\ \sin m_y \theta_y & \cos m_y \theta_y \end{bmatrix}}_{\text{vertical}} = \begin{bmatrix} \cos(m_x \theta_x + m_y \theta_y) & -\sin(m_x \theta_x + m_y \theta_y) \\ \sin(m_x \theta_x + m_y \theta_y) & \cos(m_x \theta_x + m_y \theta_y) \end{bmatrix}. \quad (9)$$

The attention score computation yields:

$$\begin{aligned} q'_{m_x, m_y} &= q_{m_x, m_y} \begin{bmatrix} \cos(m_x \theta_x + m_y \theta_y) & -\sin(m_x \theta_x + m_y \theta_y) \\ \sin(m_x \theta_x + m_y \theta_y) & \cos(m_x \theta_x + m_y \theta_y) \end{bmatrix}, \\ k'_{n_x, n_y} &= k_{n_x, n_y} \begin{bmatrix} \cos(n_x \theta_x + n_y \theta_y) & -\sin(n_x \theta_x + n_y \theta_y) \\ \sin(n_x \theta_x + n_y \theta_y) & \cos(n_x \theta_x + n_y \theta_y) \end{bmatrix}, \\ q'_{m_x, m_y} (k'_{n_x, n_y})^\top &= q_m \begin{bmatrix} \cos \theta_{(m_x - n_x, m_y - n_y)} & -\sin \theta_{(m_x - n_x, m_y - n_y)} \\ \sin \theta_{(m_x - n_x, m_y - n_y)} & \cos \theta_{(m_x - n_x, m_y - n_y)} \end{bmatrix} k_n^\top, \end{aligned} \quad (10)$$

where $\theta_{(m_x - n_x, m_y - n_y)} = (m_x - n_x)\theta_x + (m_y - n_y)\theta_y$ encodes relative positions. Due to the ambiguity in defining relative importance of horizontal versus vertical positional dependencies, we make angles θ_x and θ_y learnable, initializing them to 10000 following original RoPE [63].

3.4.4. GUIDED SELECTIVE COMPRESSION

Zero-centered quantization in Equation 5 produces many zero elements in $\lceil \Lambda \rceil = \lceil y - \mu \rceil$, as illustrated in Figure 5. While these zeros consume minimal bit rate, they account for significant arithmetic encoding/decoding time.

Recent selective compression methods [2, 39] have employed neural networks to predict selective compression maps, but they are primarily applied to simpler entropy models. In addition, scale-based prediction has been introduced in recent works [62, 84]. However, when extended to advanced entropy models [33, 34], *the training phase becomes highly unstable, with the overall loss value becoming “nan” after several steps, regardless of whether the parameters of the compression model are frozen or not.* The observed training instability is primarily caused by the dependency introduced by the context modeling, rather than by the selective compression mechanism itself. Specifically, skipping non-zero elements in the current slice can significantly affect the entropy modeling of subsequent slices due to the inter-latent dependencies established by the context model. Considering the substantial performance gains enabled by context modeling, our goal is to skip the

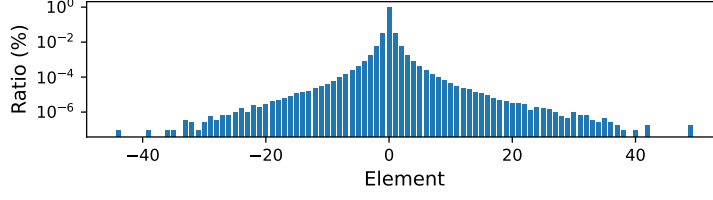


Figure 5: Ratios of different elements in $[\Lambda] = [y - \mu]$ when the model is optimized for MSE and the $\lambda = 0.013$. There are many zero elements in $[\Lambda]$.

encoding of zero elements as much as possible—on top of the existing context modeling framework [30, 33, 34, 51]—in order to reduce the time spent on arithmetic encoding and decoding.

To address above issues, the guided selective compression module f_s is proposed for post-training. This module is employed on the converged MLICv2, with the weights of MLICv2 frozen for stable training. The architecture of the guided selective compression f_s module is presented in Fig. 2. Specifically, in f_s , the scale-based selective prediction is employed as the initial predicted selective compression map. For j -th element $s_{\sigma,j}$ in s_{σ} , the scale-based selective compression value is:

$$s_{\sigma,j} = \begin{cases} 0, & \sigma_j < \xi, \\ 1, & \sigma_j \geq \xi, \end{cases} \quad (11)$$

where ξ is a predefined threshold, set to 0.3. For y_{ac}^i , the decoded elements of previous slices serve as priors. For y_{na}^i , the decoded elements of previous slices and y_{ac}^i serve as priors. The hyperprior \hat{H} also serves as a prior. The predicted selective map is formulated as:

$$\begin{aligned} \epsilon_{ac}^i &= f_s \left(s_{\sigma,ac}^i, [\Lambda^{<i}] \odot s^{<i}, \hat{H} \right), s_{ac}^i = \text{STE} \left(\text{Sigmoid} \left(\epsilon_{ac}^i \right) \right), \\ \epsilon_{na}^i &= f_s \left(s_{\sigma,na}^i, [\Lambda^{<i}] \odot s^{<i}, [\Lambda_{ac}^i] \odot s_{ac}^i, \hat{H} \right), s_{na}^i = \text{STE} \left(\text{Sigmoid} \left(\epsilon_{na}^i \right) \right). \end{aligned} \quad (12)$$

During training, $[\Lambda]$ is known, therefore cross-entropy loss is employed to optimize f_s , treating selective prediction as a *binary classification* task. Additionally, elements with larger values have a higher impact on distortion, so the cross-entropy loss is weighted by $[\Lambda] + 1$. To the best of our knowledge, we are the *first* to highlight the importance of quantization residuals and incorporate a weighted loss accordingly. The overall loss is:

$$\begin{aligned} \mathcal{L}_s &= \sum_{i=0}^L \left(([\Lambda_{ac}^i] + 1) \odot \mathcal{L}_{ce,ac}^i + ([\Lambda_{na}^i] + 1) \odot \mathcal{L}_{ce,na}^i \right), \\ \mathcal{L}_{ce,ac}^i &= - \frac{[\Lambda_{ac}^i] \odot \log \epsilon_{ac}^i + (1 - [\Lambda_{ac}^i]) \odot \log(1 - \epsilon_{ac}^i)}{2}, \\ \mathcal{L}_{ce,na}^i &= - \frac{[\Lambda_{na}^i] \odot \log \epsilon_{na}^i + (1 - [\Lambda_{na}^i]) \odot \log(1 - \epsilon_{na}^i)}{2}. \end{aligned} \quad (13)$$

3.5. Iterative Latent Refinement

To validate our MLICv2’s potential and demonstrate achievable performance improvements, we employ *encoding-time scaling* to find optimal quantized latent representation \hat{y} and side information \hat{z} for each input. Direct encoder optimization requires storing model weights, gradients and intermediate features, leading to prohibitive memory consumption for high-resolution images. We adopt Stochastic Gumbel Annealing (SGA) [80] to refine y and z efficiently. In SGA, outputs of g_a and h_a serve as initialization. For anchor part y_{ac}^i , $\Lambda_{ac}^i = y_{ac}^i - \mu_{ac}^i$ is stochastically rounded up or down. The stochastic rounding direction is sampled from a relaxed one-hot categorical distribution:

$$q_{\tau}(\mathbf{o}_{ac}^i | \Lambda_{ac}^i) \propto \begin{cases} \exp \left\{ \frac{-\text{atanh}(\Lambda_{ac}^i - \lfloor \Lambda_{ac}^i \rfloor)}{\tau} \right\}, & \mathbf{o}_{ac}^i = \{0, 1\}, \\ \exp \left\{ \frac{-\text{atanh}(\lceil \Lambda_{ac}^i \rceil - \Lambda_{ac}^i)}{\tau} \right\}, & \mathbf{o}_{ac}^i = \{1, 0\}, \end{cases} \quad (14)$$

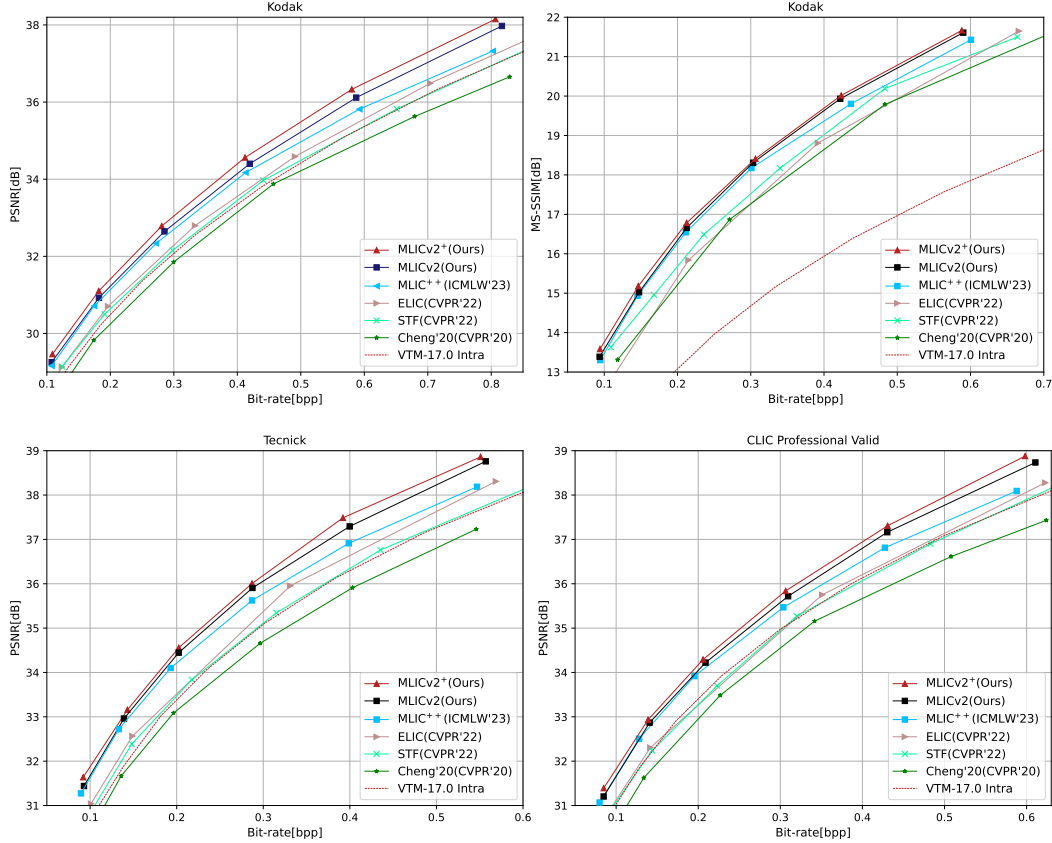


Figure 6: PSNR-Bit-rate curve and MS-SSIM-Bit-rate curve. MS-SSIM is converted to dB for better visual clarity. Please zoom in for better view.

where temperature $\tau = \min(0.5, e^{0.001j})$ decreases with refinement step j , gradually making the latent representation aware of quantization. Notably, selective compression is not incorporated during SGA. Instead, the selective compression map is predicted by f_s based on the overfitted latent representations obtained after SGA. we primarily employ it as a validation tool to demonstrate our model’s potential for instance-level adaptability and performance improvements. Rate control mechanisms [84] could be incorporated in future work for applications requiring strict bit-rate constraints.

4. Experiments

4.1. Implementation Details

4.1.1. TRAINING DATASET

Our training dataset contains 101,104 images with resolutions exceeding 640×640 pixels. These images are carefully selected from various established image datasets [1, 18, 42, 43, 77]. To address the existing compression artifacts in JPEG images, we follow the approach of Ballé *et al.* [10] by further down-sampling the JPEG images using a randomized factor. Additionally, images with bits per pixel (bpp) lower than 3 are excluded to ensure data quality.

4.1.2. TRAINING STRATEGY

MLICv2 is implemented using PyTorch 2.2.2 and CompressAI 1.2.6. Following CompressAI, we configure $\lambda \in \{18, 35, 67, 130, 250, 483\} \times 10^{-4}$ for MSE optimization and $\lambda \in \{2.4, 4.58, 8.73, 16.64, 31.73, 60.5\}$ for Multi-Scale Structural Similarity (MS-SSIM) [73]. Training is conducted on eight Tesla A100-80G GPUs with a batch size of 16, employing the Adam optimizer $\beta_1 = 0.9, \beta_2 = 0.999$. Our training consists of two stages: *Stage 1*: We train the model with only hyperprior for 2 million (M) steps using a learning rate of 10^{-4} and 256×256 patches, providing superior initialization

MLICv2: Enhanced Multi-Reference Entropy Modeling for Learned Image Compression

Methods	Venue	BD-Rate (%) w.r.t. VTM 17.0 Intra			
		PSNR	Kodak MS-SSIM	Tecnick PSNR	CLIC Pro Valid PSNR
Cheng'20 [16]	CVPR'20	5.58	-44.21	7.57	11.71
ChARM [51]	ICIP'20	3.23	—	-0.88	—
Qian'21 [55]	ICLR'21	10.05	-39.53	7.52	0.02
Xie'21 [75]	ACMMM'21	1.55	-43.39	-0.80	3.21
NLAIC'21 [15]	TIP'21	11.80	-40.27	7.11	—
Gao'21 [24]	ICCV'21	-8.76	-48.60	-	-6.49
Guo'22 [26]	TCSVT'22	-4.45	-45.23	—	—
LBHIC [74]	TCSVT'22	-4.56	-50.54	—	—
Entroformer [54]	ICLR'22	4.73	-42.64	2.31	-1.04
SwinT-ChARM [87]	ICLR'22	-1.73	—	—	—
NeuralSyntax [71]	CVPR'22	8.97	-39.56	—	5.64
STF [88]	CVPR'22	-2.48	-47.72	-2.75	0.42
WACNN [88]	CVPR'22	-2.95	-47.71	-5.09	0.04
ELIC [30]	CVPR'22	-5.95	-44.60	-9.14	-3.45
Contextformer [38]	ECCV'22	-5.77	-46.12	-9.05	—
GLLMM [22]	TIP'23	-1.43	-47.41	-5.58	—
NVTC [21]	CVPR'23	-1.04	—	—	—
LIC-TCM Large [45]	CVPR'23	-10.14	-48.94	-11.47	-8.04
QARV [19]	TPAMI'24	0.31	—	-3.03	-
FTIC [40]	ICLR'24	-12.99	-51.13	-14.88	-9.53
LLIC-TCM [32]	TMM'24	-10.94	-49.73	-14.99	-10.41
WeConvne [23]	ECCV'24	-6.71	-48.63	-8.42	-5.74
CCA [27]	NeurIPS'24	-12.04	—	-14.55	-10.75
MambaIC [82]	CVPR'25	-13.03	—	-18.41	-15.58
LALIC [20]	CVPR'25	-13.72	-50.86	-18.19	-14.34
DCAE [47]	CVPR'25	-15.43	-53.20	-20.51	-15.78
Baseline Models					
MLIC [34]	ACMMM'23	-8.05	-49.13	-12.73	-8.79
MLIC ⁺ [34]	ACMMM'23	-11.39	-52.75	-16.38	-12.56
MLIC ⁺⁺ [33]	ICMLW'23	-13.39	-53.63	-17.59	-13.08
MLICv2	Ours	-16.54	-54.56	-21.61	-16.05
MLICv2 ⁺	Ours	-20.46	-55.86	-24.35	-19.14

Table 1: BD-Rate (%) comparison for PSNR (dB) and MS-SSIM. The anchor is VTM-17.0 Intra. “—” means the result is not available.

for analysis and synthesis transforms. *Stage 2*: Loading the pre-trained weights, we train the complete model for 2M steps. The learning rate follows a scheduled decay: starting at 10^{-4} , then decreasing to 3×10^{-5} , 10^{-5} , 3×10^{-6} and 10^{-6} , at 1.5M, 1.8M, 1.9M, and 1.95M steps, respectively. We employ 256×256 patches for the initial 1.2M steps, then transition to 512×512 patches to leverage the effectiveness of global context modules. For the guided selective compression module optimization, we conduct 20K steps with batch size 16 and learning rate 10^{-3} .

To validate our model’s potential for further improvement, we employ SGA in MLICv2⁺, refining latent representations and side information for 3000 steps with learning rate 10^{-3} . This approach allows us to further enhance the performance under our architectural framework.

4.2. Benchmarks and Metrics

We evaluate rate-distortion performance on three datasets extensively used in learned compression research [9, 10, 15, 16, 19, 26, 30, 31, 32, 33, 34, 38, 45, 50, 51, 64, 71, 74, 75, 87, 88]:

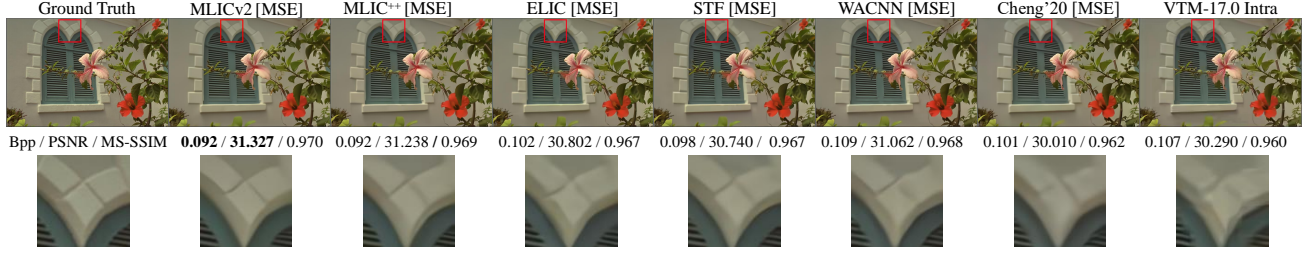


Figure 7: Reconstructions of our proposed MLICv2, recent learned image compression models [16, 30, 33, 88] and VTM-17.0 Intra [12]. “[MSE]” denotes the model is optimized for MSE. Please zoom in for better view.

- Kodak [37]: Contains 24 uncompressed images with 768×512 pixels.
- Tecnick [4]: Comprises 100 uncompressed images with 1200×1200 pixels.
- CLIC Pro Valid [65]: The validation set from the 3rd Challenge on Learned Image Compression, consisting of 41 high-resolution images with 2048×1440 pixels.

Performance ranking employs the Bjøntegaard delta rate (BD-Rate) metric [11] for comprehensive evaluation.

4.3. Rate-Distortion Performance

4.3.1. QUANTITATIVE RESULTS

For a fair comparison with learned image compression models, VTM-17.0 Intra is evaluated in YUV444 color space under *encoder.intra_vtm.cfg*. To demonstrate the superiority of our MLICv2 and MLICv2⁺, we compare with recent learned image compression models [15, 16, 20, 21, 22, 23, 26, 30, 32, 38, 40, 41, 45, 47, 51, 54, 55, 74, 75, 87, 88].

The rate-distortion curves are presented in Fig. 6. When compared with our baseline MLIC⁺⁺, MLICv2⁺ performs significantly better, especially at high bit-rates and on high-resolution images [4, 65]. Specifically, our MLICv2 achieves a maximum improvement of 0.6, 0.5, 0.5 dB when the bpp is around 0.8, 0.55, 0.6 on Kodak, Tecnick, CLIC Pro Val, respectively. Our MLICv2⁺ achieves larger improvement compared to MLIC⁺⁺ [33] due to adopted latent refinement [80] for enhanced instance adaptability. The average improvements of latent refinement on MLICv2 on Kodak [37], Tecnick [4], CLIC Pro Val [65] are 0.22, 0.15, 0.15 dB, respectively.

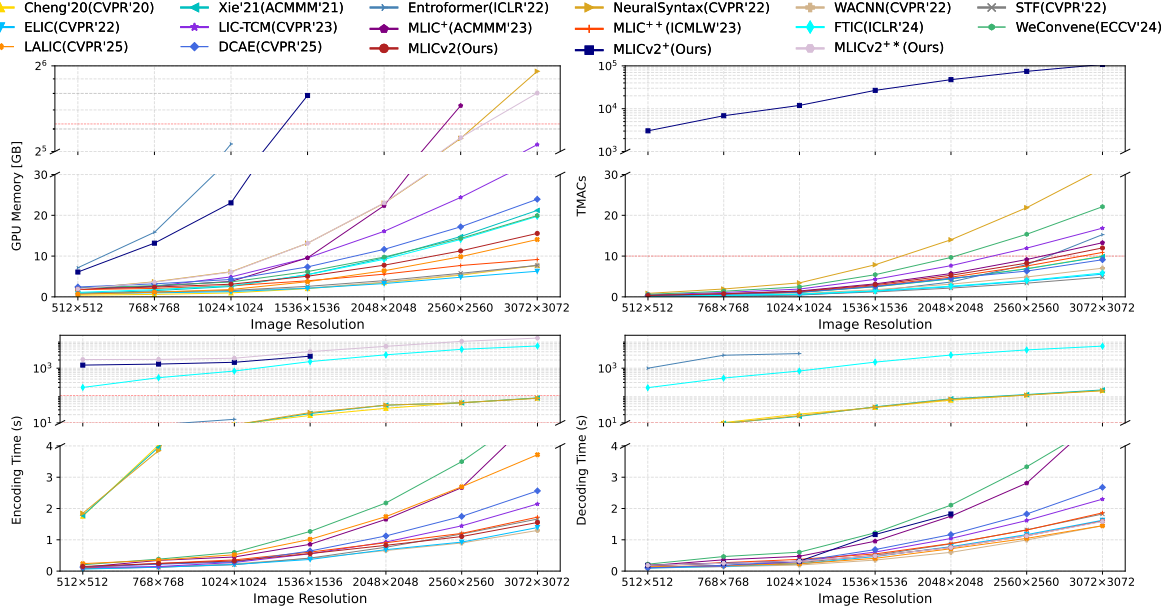
BD-Rate reductions over VTM-17.0 Intra are presented in Table 1. Compared with existing methods, our MLICv2 and MLICv2⁺ achieve state-of-the-art performance, reducing BD-Rates by 16.54% and 20.46% on Kodak. When compared to the baseline model MLIC⁺⁺ [33], our MLICv2 and MLICv2⁺ reduce 3.15% and 7.07% more bit-rates over VTM-17.0 Intra on Kodak [37], respectively. Our MLICv2 and MLICv2⁺ also achieve superior performances on high-resolution datasets Tecnick [4] and CLIC Pro Val [65]. Specifically, our MLICv2 and MLICv2⁺ reduce BD-Rates by 21.61% and 24.35% on Tecnick [4] and 16.05% and 19.14% on CLIC Pro Val [65].

4.3.2. QUALITATIVE RESULTS

We also compare the qualitative performance to MLIC⁺⁺, ELIC [30], STF, WACNN [88], Cheng’20 [16] and VTM-17.0 Intra on subjective qualities. The windowsill of reconstructions are cropped to patches for clearer comparisons. The reconstructions of MLICv2 have sharper textures and retain more details. In terms of visual quality, our MLICv2 has significant improvements on rate-perception performance compared to other models.

4.4. Computational Complexity

The model complexities and sizes are presented in Fig. 8 and Table 5, respectively. To comprehensively evaluate model complexity, 16 images from the LIU4K dataset [44] are cropped to $\{512 \times 512, 768 \times 768, 1024 \times 1024, 1536 \times 1536, 2048 \times 2048, 2560 \times 2560, 3072 \times 3072\}$ patches to cover the various resolutions of images that can be encountered in practical scenarios. Forward GPU memory, encoding time, decoding time, and forward Multiply-Accumulate operations (MACs) are employed as the complexity metrics. Encoding and decoding times include arithmetic encoding and decoding times.



- (1) In MLICv2⁺⁺, gradient checkpointing [14] is employed during the SGA iterations.
- (2) The MACs of MLICv2⁺ are theoretically estimated based on the number of SGA iterations, following the observation from Epoch AI that backward and forward passes almost always have MAC ratios close to 2:1². The MACs of MLICv2⁺⁺ are not reported due to the use of gradient checkpointing, which prevents accurate profiling.
- (3) The lack of reported results for some models at certain resolutions is due to out-of-memory (OOM) issues or inaccurate profiling.

Figure 8: GPU memory consumption, Forward MACs, encoding time and decoding time comparisons among our proposed models and recent learned image compression models [16, 30, 33, 34, 40, 45, 71, 75, 88].

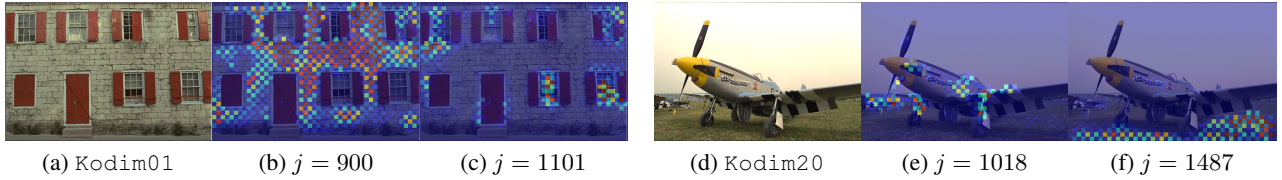


Figure 9: Visualization of attention maps of hyperprior guided intra slice global context module. The inputs are Kodim01 and Kodim20. The attention map is computed by $\text{Softmax}_2(\hat{H}_{na,q})[j]\text{Softmax}_1(\hat{H}_{ac,k})^\top$, where j is the query index.

Since the number of skipped elements at different bit-rates varies, we report the results of MLICv2 and MLICv2⁺ with $\lambda = 0.0130$.

Due to the high memory consumption introduced by SGA, we employ gradient checkpointing [14] to overcome GPU memory limitations. This technique alleviates memory pressure by selectively recomputing a subset of intermediate activations during the backward pass. Instead of storing all intermediate activations during the forward pass, only a small set—typically those essential for gradient computation—are cached. The remaining activations are recomputed on-the-fly during backpropagation. This strategy significantly reduces peak memory usage, albeit at the cost of increased computation time.

4.4.1. ON FORWARD GPU MEMORY

Compared to MLIC⁺[34], MLICv2 significantly reduces memory usage thanks to its linear-complexity entropy model. Relative to MLIC⁺⁺[33], it incurs slightly higher memory for high-resolution images due to the additional modules introduced in this work, but still requires less memory than Xie'21 [75], Qian'21 [55], Entroformer [55], and LIC-TCM [45].

¹<https://epoch.ai/blog/backward-forward-FLOP-ratio>

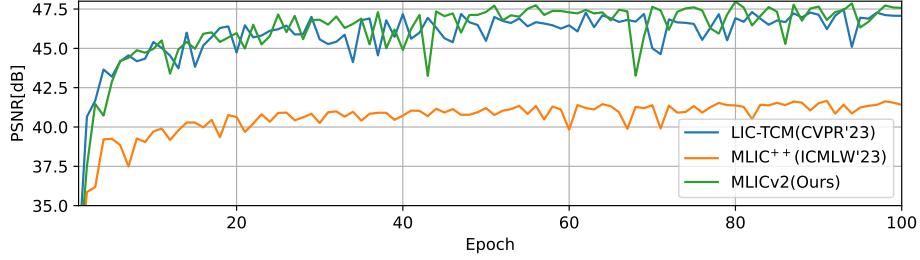


Figure 10: Upper-bound reconstruction quality (PSNR) on the Kodak dataset without entropy constraints.

Transform Architecture	Cheng'20 [16]	SwinT [87]	ELIC [30]	MLIC ⁺⁺	LIC-TCM [45]	MLICv2
BD-Rate(%)	0.00	-4.61	-5.19	-0.41	-8.91	-9.44

Table 2: Comparisons among different transforms of proposed MLICv2, LIC-TCM [45], MLIC⁺⁺, ELIC [30], and Cheng'20 [16]. All method are quiped with autoregressive context module [52].

This modest increase is justified by the corresponding performance improvements. Latent refinement, while increasing memory during backpropagation, is optional and primarily benefits scenarios where encoding complexity is less critical. Since images are typically encoded once but decoded multiple times, the added encoding cost is acceptable given the notable gains in rate-distortion performance.

4.4.2. ON FORWARD MACS

Compared to MLIC⁺, LIC-TCM [45], our MLICv2 has lower forward MACs. Compared to MLIC⁺⁺, our MLICv2 exhibits slightly higher forward MACs. This increase can be attributed to two primary factors: the proposed channel reweighting module and selective compression module. However, considering the significant performance gains achieved through these enhancements, the marginal increase in MACs is deemed acceptable. The trade-off between computational complexity and improved compression efficiency is well-balanced in our proposed model.

4.4.3. ON ENCODING TIME AND DECODING TIME

Compared to MLIC and MLIC⁺ [34], MLICv2 achieves higher encoding and decoding efficiency due to its linear-complexity components. Relative to MLIC⁺⁺ [33], it further reduces encoding and decoding time by efficiently skipping many zero elements, which is particularly beneficial for high-resolution images where zeros are more frequent. Latent refinement, while involving multiple backpropagation steps and increasing encoding time, is optional and suited for scenarios where encoding complexity is less critical. Since images are typically encoded once but decoded multiple times, the extra encoding cost is justified by the performance gains. Notably, MLICv2⁺ maintains decoding complexity nearly identical to MLICv2, with both substantially faster than MLIC⁺⁺, recent WeConvene [23] and DCAE [47].

4.4.4. ON MODEL SIZE

The model size comparisons are presented in Table 5. Although MLICv2 incorporates several additional components, its parameter count (84.3M) remains comparable to that of MLIC⁺⁺ (83.5M). The increase in parameters is minimal, primarily because we deliberately reduce the number of channels for intermediate features in the context modules of MLICv2 to control overall model size.

4.5. Ablation Studies

4.5.1. SETTINGS

Each ablation cases is optimized for MSE using our established training strategy, with MLICv2⁺ serving as the anchor. We evaluate both cumulative benefits and individual contributions of each proposed component. The results are presented in Table 4.

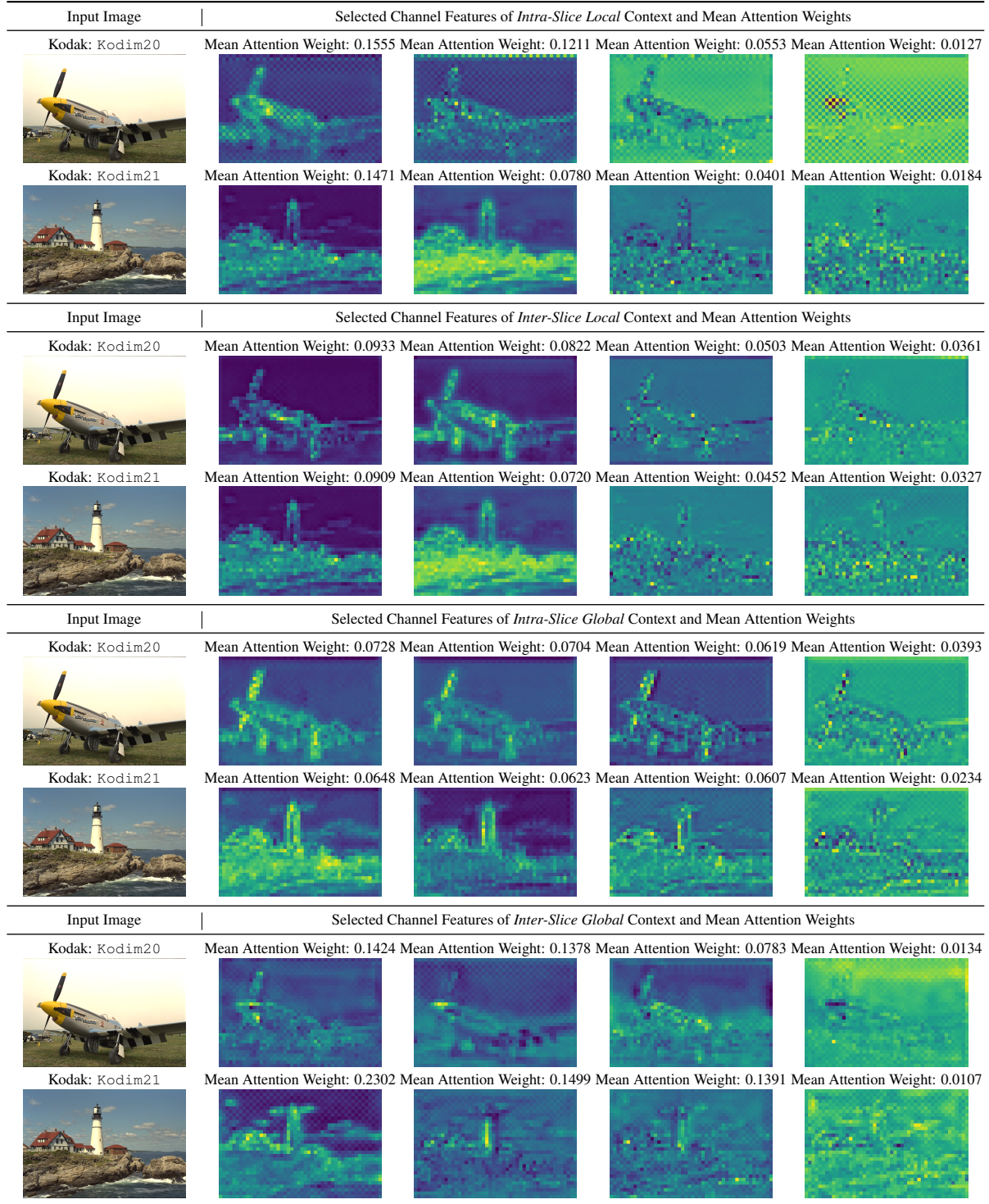


Figure 11: Visualization of selected channel features and their corresponding Mean Attention Weights. All channels are sampled from the context features (before context reweighting) of the last slice. The visualized feature maps are normalized to the range $[0, 1]$.

MLICv2: Enhanced Multi-Reference Entropy Modeling for Learned Image Compression

Context Module	MLIC ⁺⁺	MLICv2	Hyperprior	Guided Global Context	2D RoPE	Context Reweighting	Selective Compression
GMACs	508.49	506.76		1.62	2.4×10^{-5}	3.46	1.73

Table 3: MACs contribution of the introduced modules to the entropy model on the Kodak dataset

Context Modules	MLICv2 ⁺	Cumulative Benefits								Individual Contributions							
	Full	Case 1	Case 2	Case 3	Case 4	Case 5	Case 6	Case 7	Case 8	Case 9	Case 10	Case 11	Case 12	Case 13	Case 14	Case 15	Case 16
Latent Refinement	✓	✓								✓							
Selective Compression	✓		✓								✓						
2D RoPE	✓	✓	✓	✓								✓					
Context Reweighting	✓	✓	✓	✓	✓								✓				
Hyperprior Guided Global	✓	✓	✓	✓	✓	✓								✓			
Simple Token Mixing Transform	✓	✓	✓	✓	✓	✓	✓									✓	
Gate	✓	✓	✓	✓	✓	✓	✓	✓									✓
BD-Rate (%)	0.00	0.17	4.89	5.21	5.77	7.79	8.29	9.58	9.87	4.64	9.52	9.12	7.64	8.77	8.51	9.58	9.87

Table 4: Complete ablation study on Kodak dataset. BD-Rate (%) is employed to evaluate component contributions. MLICv2⁺ is the anchor. Cases 1-8 show cumulative benefits, Cases 9-16 show individual contributions.

4.5.2. ANALYSIS OF ENHANCED TRANSFORM

To demonstrate the superior capacity of our proposed transform, we compare the upper bounds of reconstruction quality achieved by the transforms in MLIC⁺⁺ [33], LIC-TCM [45], and our MLICv2. The results are shown in Fig. 10. Our MetaFormer-based design achieves better reconstruction quality than MLIC⁺⁺ and performs comparably to LIC-TCM, highlighting its stronger representational power despite relying primarily on convolutional operations.

To demonstrate the effectiveness of the proposed simple token mixing block, we compare the transform module with the transform modules of Cheng’20 [16], SwinT-Charm [87], ELIC [30], and LIC-TCM [45] on rate-distortion performance. The entropy model is aligned with spatial autoregressive entropy model [50]. The results are presented in Table. 2. Our proposed transform achieves better performance than LIC-TCM while with about half forward MACs. When equipped with proposed transform, the model performance gets further enhanced. Since our baseline performance is very strong, the boost from the transform is slightly small relative to Table. 2.

4.5.3. ANALYSIS OF ENHANCED ENTROPY MODELING

As shown in Table 4, disabling the selective compression module results in a 0.17% performance drop, which is acceptable, as the skipped elements—primarily zeros—typically have very low entropy despite accounting for the majority of all latent elements. By omitting the encoding of these zero elements, we can significantly accelerate both arithmetic encoding and decoding. To demonstrate the effectiveness of proposed guided selective compression on acceleration, the skip ratio, encoding acceleration and decoding acceleration on Kodak [37] and CLIC Pro Val [65] are presented in Table 6. As image quality improves, the proportion of zero elements that can be skipped decreases, which in turn reduces the acceleration gains for both encoding and decoding. However, high-resolution images usually contain more redundancy, allowing a larger number of elements to be skipped. This leads to greater potential for acceleration in such cases. In addition, we found that setting ξ to 0.2, 0.3, or 0.4 has little effect on overall performance. This is mainly due to two reasons. First, as illustrated in Figure 12, most scale values fall within the range [0.1, 0.2], with only a small fraction between 0.2 and 0.4. Thus, using ξ within this range is already effective in skipping most zero elements with low prediction error. The selective compression module only needs to correct a few wrongly skipped important elements. Second, we apply a weighted binary classification loss to train the selective compression module, using the ground-truth encoding mask as supervision.

To demonstrate the effectiveness of hyperprior-guided global context for the first slice, the attention maps are illustrated in Fig. 9, which are generally accurate, thereby enhancing the performance. For slices $\hat{y}^{\geq 1}$, the previous one slice is still employed to predict the global correlations due to the higher bit-rate of each slice compared to the side information.

To demonstrate the relationship between context reweighting map and image content, we visualize the Mean Attention Weight in Fig. 11.

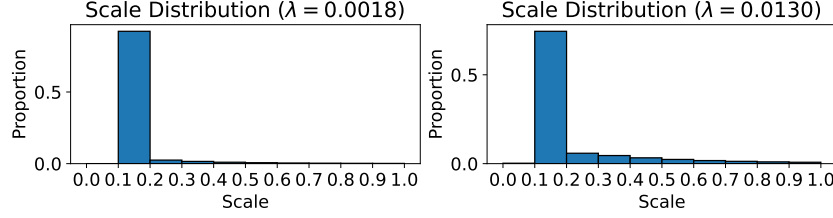


Figure 12: Distribution of scale values in MLICv2 on Kodak [37].

Model	Xie'21 [75]	ELIC [30]	WACNN [88]	STF [88]	LIC-TCM [45]	FTIC [40]	MLIC ⁺ [34]	MLIC ⁺⁺ [33]	WeConvne [23]	LALIC [20]	DCAE [47]	MLICv2
Parameters (M)	50.0	41.9	75.2	100.0	75.9	69.8	83.4	83.5	105.5	63.2	119.2	84.3

Table 5: Model Size Comparison.

Definition 4.1 (Mean Attention Weight). In the channel reweighting module, the attention map is computed as $M = \text{Softmax}(Q^T K) \in \mathbb{R}^{C \times C}$, where C is the number of channels. The attention map is row-wise normalized via the Softmax function: $M_{i,j} = \frac{\exp(q_i^T k_j)}{\sum_{j^*=1}^C \exp(q_i^T k_{j^*})}$, where q_i and k_j are the i -th and j -th channel vectors of Q and K , respectively. This normalization ensures that each row of M sums to 1, meaning that $M_{i,j}$ reflects the relative influence of input channel j on output channel i when computing the weighted sum: $o_i = \sum_{j=1}^C M_{i,j} v_j$, where v_j is j -th channel vector V . The Mean Attention Weight for each input channel j is then defined as the average over the j -th column of M : $\tilde{M}_j = \frac{1}{C} \sum_{i=1}^C M_{i,j}$, which reflects the overall influence of input channel j across all output channels.

As observed, channels dominated by noise tend to receive lower Mean Attention Weight, while those containing richer structural information or less noise are assigned higher weight. This demonstrates that our context reweighting module effectively emphasizes more informative contexts, supporting its contribution to the performance gains.

To validate the effectiveness of the proposed 2D RoPE, the 2D RoPE is replaced by original additive relative position embedding [46]. The performance degradation caused by the replacement demonstrates the superiority of the proposed 2D RoPE. Inspired by some 2D positional encoding designs [13, 57, 72], which split the feature tensor along the channel dimension and apply positional encoding along the horizontal axis to one half and the vertical axis to the other, we also experimented with a similar strategy. Specifically, we divided the input tensor along the channel dimension into two parts and applied RoPE-based rotations along the horizontal axis and vertical axis, respectively. We found that this alternative design does not lead to a performance difference. We also conduct experiments on the baseline model using 2D RoPE *without* learnable θ_x and θ_y . This variant results in approximately a 0.4% performance drop.

To validate the effectiveness of the gate block, the gate block is replaced by Multilayer Perceptron (MLP), which leads to performance loss.

Overall, the newly introduced modules in the entropy model yield substantial performance gains with minimal additional computational cost, as demonstrated in our ablation studies and Table 3. As reported in Table 3, the MACs of 2D RoPE are almost negligible. The context reweighting and selective compression modules contribute only 0.68% and 0.34% to the total MACs on the Kodak dataset, respectively. This efficiency is largely due to the fact that the proposed modules for entropy modeling operate in the latent space, where the spatial resolution is only $\frac{1}{16} \times \frac{1}{16}$ of the input image. *Such a drastic reduction in resolution greatly reduces the overall computational burden.*

4.5.4. ANALYSIS OF ITERATIVE LATENT REFINEMENT

In case 1, the latent refinement is removed, which leads to around 4.89% bit-rate increase compared to MLICv2⁺. The increased bit-rate demonstrates the effectiveness of the latent refinement for exploring performance potential. The changes of loss, PSNR and bpp are illustrated in Fig. 13. During the refinement, the loss and bpp generally first rise and then fall to

λ	Kodak						CLIC Pro Val					
	0.0018	0.0035	0.0067	0.0130	0.0250	0.0483	0.0018	0.0035	0.0067	0.0130	0.0250	0.0483
Skip Ratio (%)	88.32	82.73	77.09	69.76	66.44	57.26	92.95	88.20	83.72	79.72	77.28	68.81
Enc Acceleration (%)	9.98	9.48	9.24	8.81	7.31	7.22	18.48	17.12	16.88	16.62	16.15	14.21
Dec Acceleration (%)	13.61	13.21	12.15	11.97	10.18	9.62	27.52	25.85	25.37	24.21	23.36	20.99

Table 6: Skip Ratio, Encoding Acceleration and Decoding Acceleration at different qualities on Kodak and CLIC Pro Val.

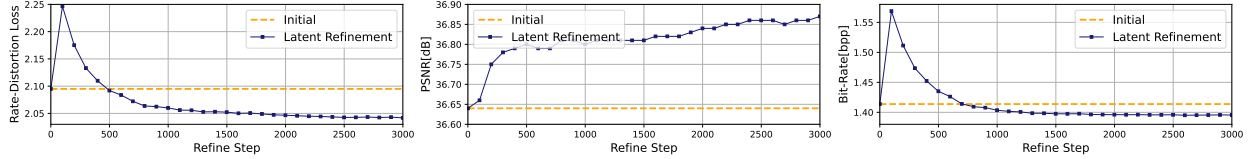


Figure 13: Changes in loss, PSNR and bpp during the refinement of latent representation and side information of Kodim01 from Kodak dataset [37]. “Initial” denotes the original loss, psnr, bpp when using the latent representation and side information outputted by MLICv2.

lower than the initial loss and bpp, while the PSNR generally keeps rising.

5. Conclusion

In this paper, we present MLICv2 and MLICv2⁺, enhanced versions of the previous MLIC series that address observed limitations in transform design and entropy modeling. To overcome these limitations, we introduce efficient simple token mixing blocks that substantially improve representational capacity while maintaining computational efficiency. Our MetaFormer-based design achieves comparable performance to complex transformer alternatives with reduced overhead. For entropy modeling, we propose hyperprior-guided global context prediction, context reweighting mechanisms, and novel 2D Rotary Positional Embedding, collectively providing richer contextual information. The guided selective compression further accelerates encoding/decoding through intelligent zero-element skipping. Additionally, by employing SGA, we demonstrate the potential for performance improvements within our architectural framework. This validation analysis reveals the potential for further architectural improvements and provides valuable insights for future development directions. These innovations collectively establish new state-of-the-art performance benchmarks, with BD-Rate reductions of up to 20% compared to VTM-17.0 Intra while maintaining competitive computational complexity. Furthermore, to continue exploring the performance upper bounds via encoding-time scaling, we plan to investigate the transmission of update parameters [49, 59, 67] to the decoder side.

Limitations: Although our MLICv2 and MLICv2⁺ achieve state-of-the-art performance, several limitations warrant future attention. First, the performance potential exploration through SGA may lead to bitrate variations [84], requiring practical online encoder optimization strategies for precise bitrate control. Second, MLICv2/MLICv2⁺ may encounter cross-platform decoding issues [7, 29, 61, 79]. We plan to investigate model quantization techniques [28, 29, 61] and chain coding-based latent compression [79] to address deployment challenges.

References

- [1] Eirikur Agustsson and Radu Timofte. Ntire 2017 challenge on single image super-resolution: Dataset and study. *Proceedings of the IEEE/CVF Conference on Computer Vision and Pattern Recognition Workshops*, pages 1122–1131, 2017.
- [2] David Alexandre, Hsueh-Ming Hang, and Wen-Hsiao Peng. Hierarchical b-frame video coding using two-layer canf without motion coding. In *Proceedings of the IEEE/CVF Conference on Computer Vision and Pattern Recognition*, pages 10249–10258, 2023.
- [3] Alaaeldin Ali, Hugo Touvron, Mathilde Caron, Piotr Bojanowski, Matthijs Douze, Armand Joulin, Ivan Laptev, Natalia

- Neverova, Gabriel Synnaeve, Jakob Verbeek, et al. Xcit: Cross-covariance image transformers. *Advances in Neural Information Processing Systems*, 34:20014–20027, 2021.
- [4] N. Asuni and A. Giachetti. Testimages: a large-scale archive for testing visual devices and basic image processing algorithms. In *Smart Tools and Apps for Graphics*, 2014.
- [5] Jimmy Lei Ba, Jamie Ryan Kiros, and Geoffrey E Hinton. Layer normalization. *arXiv:1607.06450*, 2016.
- [6] Johannes Ballé, Philip A Chou, David Minnen, Saurabh Singh, Nick Johnston, Eirikur Agustsson, Sung Jin Hwang, and George Toderici. Nonlinear transform coding. *IEEE Journal of Selected Topics in Signal Processing*, 15(2):339–353, 2020.
- [7] Johannes Ballé, Nick Johnston, and David Minnen. Integer networks for data compression with latent-variable models. In *Proceedings of the International Conference on Learning Representations*, 2019.
- [8] Johannes Ballé, Valero Laparra, and Eero P Simoncelli. Density modeling of images using a generalized normalization transformation. *Proceedings of the International Conference on Learning Representations*, 2015.
- [9] Johannes Ballé, Valero Laparra, and Eero P Simoncelli. End-to-end optimized image compression. In *Proceedings of the International Conference on Learning Representations*, 2017.
- [10] Johannes Ballé, David Minnen, Saurabh Singh, Sung Jin Hwang, and Nick Johnston. Variational image compression with a scale hyperprior. In *Proceedings of the International Conference on Learning Representations*, 2018.
- [11] Gisle Bjontegaard. Calculation of average psnr differences between rd-curves. *ITU SG16 Doc. VCEG-M33*, 2001.
- [12] Benjamin Bross, Ye-Kui Wang, Yan Ye, Shan Liu, Jianle Chen, Gary J. Sullivan, and Jens-Rainer Ohm. Overview of the versatile video coding (vvc) standard and its applications. *IEEE Transactions on Circuits and Systems for Video Technology*, 31(10):3736–3764, 2021.
- [13] Nicolas Carion, Francisco Massa, Gabriel Synnaeve, Nicolas Usunier, Alexander Kirillov, and Sergey Zagoruyko. End-to-end object detection with transformers. In *Proceedings of the European Conference on Computer Vision*, pages 213–229. Springer, 2020.
- [14] Tianqi Chen, Bing Xu, Chiyuan Zhang, and Carlos Guestrin. Training deep nets with sublinear memory cost. *arXiv:1604.06174*, 2016.
- [15] Tong Chen, Haojie Liu, Zhan Ma, Qiu Shen, Xun Cao, and Yao Wang. End-to-end learnt image compression via non-local attention optimization and improved context modeling. *IEEE Transactions on Image Processing*, 30:3179–3191, 2021.
- [16] Zhengxue Cheng, Heming Sun, Masaru Takeuchi, and Jiro Katto. Learned image compression with discretized gaussian mixture likelihoods and attention modules. In *Proceedings of the IEEE/CVF Conference on Computer Vision and Pattern Recognition*, June 2020.
- [17] Ze Cui, Jing Wang, Shangyin Gao, Tiansheng Guo, Yihui Feng, and Bo Bai. Asymmetric gained deep image compression with continuous rate adaptation. In *Proceedings of the IEEE/CVF Conference on Computer Vision and Pattern Recognition*, pages 10532–10541, June 2021.
- [18] Jia Deng, Wei Dong, Richard Socher, Li-Jia Li, Kai Li, and Li Fei-Fei. Imagenet: A large-scale hierarchical image database. In *Proceedings of the IEEE/CVF Conference on Computer Vision and Pattern Recognition*, pages 248–255. IEEE, 2009.
- [19] Zhihao Duan, Ming Lu, Jack Ma, Yuning Huang, Zhan Ma, and Fengqing Zhu. Qarv: Quantization-aware resnet vae for lossy image compression. *IEEE Transactions on Pattern Analysis and Machine Intelligence*, 46(1):436–450, 2024.
- [20] Donghui Feng, Zhengxue Cheng, Shen Wang, Ronghua Wu, Hongwei Hu, Guo Lu, and Li Song. Linear attention modeling for learned image compression. In *Proceedings of the IEEE/CVF Conference on Computer Vision and Pattern Recognition*, pages 7623–7632, 2025.

- [21] Runsen Feng, Zongyu Guo, Weiping Li, and Zhibo Chen. Nvtc: Nonlinear vector transform coding. In *Proceedings of the IEEE/CVF Conference on Computer Vision and Pattern Recognition*, pages 6101–6110, June 2023.
- [22] Haisheng Fu, Feng Liang, Jianping Lin, Bing Li, Mohammad Akbari, Jie Liang, Guohe Zhang, Dong Liu, Chengjie Tu, and Jingning Han. Learned image compression with gaussian-laplacian-logistic mixture model and concatenated residual modules. *IEEE Transactions on Image Processing*, 32:2063–2076, 2023.
- [23] Haisheng Fu, Jie Liang, Zhenman Fang, Jingning Han, Feng Liang, and Guohe Zhang. Weconvene: Learned image compression with wavelet-domain convolution and entropy model. In *Proceedings of the European Conference on Computer Vision*, pages 37–53. Springer, 2024.
- [24] Ge Gao, Pei You, Rong Pan, Shunyuan Han, Yuanyuan Zhang, Yuchao Dai, and Hojae Lee. Neural image compression via attentional multi-scale back projection and frequency decomposition. In *Proceedings of the IEEE/CVF international conference on computer vision*, pages 14677–14686, 2021.
- [25] Albert Gu and Tri Dao. Mamba: Linear-time sequence modeling with selective state spaces. In *COLM*, 2024.
- [26] Zongyu Guo, Zhizheng Zhang, Runsen Feng, and Zhibo Chen. Causal contextual prediction for learned image compression. *IEEE Transactions on Circuits and Systems for Video Technology*, 32(4):2329–2341, 2022.
- [27] Minghao Han, Shiyin Jiang, Shengxi Li, Xin Deng, Mai Xu, Ce Zhu, and Shuhang Gu. Causal context adjustment loss for learned image compression. *Advances in Neural Information Processing Systems*, 37:133231–133253, 2024.
- [28] Song Han, Huizi Mao, and William J Dally. Deep compression: Compressing deep neural networks with pruning, trained quantization and huffman coding. In *Proceedings of the International Conference on Learning Representations*, 2016.
- [29] Dailan He, Ziming Yang, Yuan Chen, Qi Zhang, Hongwei Qin, and Yan Wang. Post-training quantization for cross-platform learned image compression. *arXiv:2202.07513*, 2022.
- [30] Dailan He, Ziming Yang, Weikun Peng, Rui Ma, Hongwei Qin, and Yan Wang. Elic: Efficient learned image compression with unevenly grouped space-channel contextual adaptive coding. In *Proceedings of the IEEE/CVF Conference on Computer Vision and Pattern Recognition*, June 2022.
- [31] Dailan He, Yaoyan Zheng, Baocheng Sun, Yan Wang, and Hongwei Qin. Checkerboard context model for efficient learned image compression. In *Proceedings of the IEEE/CVF Conference on Computer Vision and Pattern Recognition*, pages 14771–14780, 2021.
- [32] Wei Jiang, Peirong Ning, Jiayu Yang, Yongqi Zhai, Feng Gao, and Ronggang Wang. Llic: Large receptive field transform coding with adaptive weights for learned image compression. *IEEE Transactions on Multimedia*, pages 1–15, 2024.
- [33] Wei Jiang, Jiayu Yang, Yongqi Zhai, Feng Gao, and Ronggang Wang. Mlic++: Linear complexity multi-reference entropy modeling for learned image compression. *ACM Transactions on Multimedia Computing, Communications, and Applications*, 21(5):1–25, 2025.
- [34] Wei Jiang, Jiayu Yang, Yongqi Zhai, Peirong Ning, Feng Gao, and Ronggang Wang. Mlic: Multi-reference entropy model for learned image compression. In *Proceedings of the 31st ACM International Conference on Multimedia*, 2023.
- [35] Yili Jin, Jiahao Li, Bin Li, and Yan Lu. Neural image compression with regional decoding. *ACM Transactions on Multimedia Computing, Communications, and Applications*, 21(3):1–18, 2025.
- [36] Jun-Hyuk Kim, Byeongho Heo, and Jong-Seok Lee. Joint global and local hierarchical priors for learned image compression. In *Proceedings of the IEEE/CVF Conference on Computer Vision and Pattern Recognition*, 2022.
- [37] Eastman Kodak. Kodak lossless true color image suite, 1993.
- [38] A Burakhan Koyuncu, Han Gao, Atanas Boev, Georgii Gaikov, Elena Alshina, and Eckehard Steinbach. Contextformer: A transformer with spatio-channel attention for context modeling in learned image compression. In *Proceedings of the European Conference on Computer Vision*, pages 447–463, 2022.

- [39] Jooyoung Lee, Seyoon Jeong, and Munchurl Kim. Selective compression learning of latent representations for variable-rate image compression. *Advances in Neural Information Processing Systems*, 35:13146–13157, 2022.
- [40] Han Li, Shaohui Li, Wenrui Dai, Chenglin Li, Junni Zou, and Hongkai Xiong. Frequency-aware transformer for learned image compression. In *Proceedings of the International Conference on Learning Representations*, pages 1–11, 2024.
- [41] Mu Li, Kede Ma, Jane You, David Zhang, and Wangmeng Zuo. Efficient and effective context-based convolutional entropy modeling for image compression. *IEEE Transactions on Image Processing*, 29:5900–5911, 2020.
- [42] Bee Lim, Sanghyun Son, Heewon Kim, Seungjun Nah, and Kyoung Mu Lee. Enhanced deep residual networks for single image super-resolution. In *Proceedings of the IEEE/CVF Conference on Computer Vision and Pattern Recognition Workshops*, pages 136–144, 2017.
- [43] Tsung-Yi Lin, Michael Maire, Serge Belongie, James Hays, Pietro Perona, Deva Ramanan, Piotr Dollár, and C Lawrence Zitnick. Microsoft coco: Common objects in context. In *Proceedings of the European Conference on Computer Vision*, pages 740–755, 2014.
- [44] Jiaying Liu, Dong Liu, Wenhan Yang, Sifeng Xia, Xiaoshuai Zhang, and Yuanying Dai. A comprehensive benchmark for single image compression artifact reduction. *IEEE Transactions on Image Processing*, 29:7845–7860, 2020.
- [45] Jinming Liu, Heming Sun, and Jiro Katto. Learned image compression with mixed transformer-cnn architectures. In *Proceedings of the IEEE/CVF Conference on Computer Vision and Pattern Recognition*, 2023.
- [46] Ze Liu, Yutong Lin, Yue Cao, Han Hu, Yixuan Wei, Zheng Zhang, Stephen Lin, and Baining Guo. Swin transformer: Hierarchical vision transformer using shifted windows. In *Proceedings of the IEEE/CVF international conference on computer vision*, pages 10012–10022, October 2021.
- [47] Jingbo Lu, Leheng Zhang, Xingyu Zhou, Mu Li, Wen Li, and Shuhang Gu. Learned image compression with dictionary-based entropy model. In *Proceedings of the IEEE/CVF Conference on Computer Vision and Pattern Recognition*, pages 12850–12859, 2025.
- [48] Ming Lu, Peiyao Guo, Huiqing Shi, Chuntong Cao, and Zhan Ma. Transformer-based image compression. In *Proceedings of the Data Compression Conference*, pages 469–469, 2022.
- [49] Yue Lv, Jinxi Xiang, Jun Zhang, Wenming Yang, Xiao Han, and Wei Yang. Dynamic low-rank instance adaptation for universal neural image compression. In *Proceedings of the 31st ACM International Conference on Multimedia*, pages 632–642, 2023.
- [50] David Minnen, Johannes Ballé, and George D Toderici. Joint autoregressive and hierarchical priors for learned image compression. In *Advances in Neural Information Processing Systems*, pages 10771–10780, 2018.
- [51] David Minnen and Saurabh Singh. Channel-wise autoregressive entropy models for learned image compression. In *IEEE International Conference on Image Processing*, pages 3339–3343. IEEE, 2020.
- [52] David Minnen, George Toderici, Saurabh Singh, Sung Jin Hwang, and Michele Covell. Image-dependent local entropy models for learned image compression. In *IEEE International Conference on Image Processing*, pages 430–434. IEEE, 2018.
- [53] Jae Hyun Park, Sanghoon Kim, Joo Chan Lee, and Jong Hwan Ko. Scalable color quantization for task-centric image compression. *ACM Transactions on Multimedia Computing, Communications, and Applications*, 19(2s):1–18, 2023.
- [54] Yichen Qian, Ming Lin, Xiuyu Sun, Zhiyu Tan, and Rong Jin. Entroformer: A transformer-based entropy model for learned image compression. In *Proceedings of the International Conference on Learning Representations*, 2022.
- [55] Yichen Qian, Zhiyu Tan, Xiuyu Sun, Ming Lin, Dongyang Li, Zhenhong Sun, Li Hao, and Rong Jin. Learning accurate entropy model with global reference for image compression. In *Proceedings of the International Conference on Learning Representations*, 2020.

- [56] Shiyu Qin, Jinpeng Wang, Yimin Zhou, Bin Chen, Tianci Luo, Baoyi An, Tao Dai, Shutao Xia, and Yaowei Wang. Mambavc: Learned visual compression with selective state spaces. *arXiv:2405.15413*, 2024.
- [57] Prajit Ramachandran, Niki Parmar, Ashish Vaswani, Irwan Bello, Anselm Levskaya, and Jon Shlens. Stand-alone self-attention in vision models. *Advances in Neural Information Processing Systems*, 32, 2019.
- [58] Machel Reid, Nikolay Savinov, Denis Teplyashin, Dmitry Lepikhin, Timothy Lillicrap, Jean-baptiste Alayrac, Radu Soricut, Angeliki Lazaridou, Orhan Firat, Julian Schrittwieser, et al. Gemini 1.5: Unlocking multimodal understanding across millions of tokens of context. *arXiv:2403.05530*, 2024.
- [59] Sheng Shen, Huanjing Yue, and Jingyu Yang. Dec-adapter: Exploring efficient decoder-side adapter for bridging screen content and natural image compression. In *Proceedings of the IEEE/CVF international conference on computer vision*, pages 12887–12896, 2023.
- [60] Zhuoran Shen, Mingyuan Zhang, Haiyu Zhao, Shuai Yi, and Hongsheng Li. Efficient attention: Attention with linear complexities. In *Proceedings of the IEEE/CVF Winter Conference on Applications of Computer Vision*, 2021.
- [61] Junqi Shi, Ming Lu, and Zhan Ma. Rate-distortion optimized post-training quantization for learned image compression. *IEEE Transactions on Circuits and Systems for Video Technology*, 2023.
- [62] Yibo Shi, Yuning Ge, Jing Wang, and Jue Mao. Alphavc: High-performance and efficient learned video compression. In *Proceedings of the European Conference on Computer Vision*, pages 616–631, 2022.
- [63] Jianlin Su, Murtadha Ahmed, Yu Lu, Shengfeng Pan, Wen Bo, and Yunfeng Liu. Roformer: Enhanced transformer with rotary position embedding. *Neurocomputing*, 568:127063, 2024.
- [64] Lucas Theis, Wenzhe Shi, Andrew Cunningham, and Ferenc Huszár. Lossy image compression with compressive autoencoders. In *Proceedings of the International Conference on Learning Representations*, 2017.
- [65] George Toderici, Wenzhe Shi, Radu Timofte, Lucas Theis, Johannes Ballé, Eirikur Agustsson, Nick Johnston, and Fabian Mentzer. Workshop and challenge on learned image compression (clic2020), 2020.
- [66] Hugo Touvron, Thibaut Lavril, Gautier Izacard, Xavier Martinet, Marie-Anne Lachaux, Timothée Lacroix, Baptiste Rozière, Naman Goyal, Eric Hambro, Faisal Azhar, et al. Llama: Open and efficient foundation language models. *arXiv:2302.13971*, 2023.
- [67] Koki Tsubota, Hiroaki Akutsu, and Kiyoharu Aizawa. Universal deep image compression via content-adaptive optimization with adapters. In *Proceedings of the IEEE/CVF Winter Conference on Applications of Computer Vision*, pages 2529–2538, 2023.
- [68] Hanyue Tu, Li Li, Wengang Zhou, and Houqiang Li. Reconstruction-free image compression for machine vision via knowledge transfer. *ACM Transactions on Multimedia Computing, Communications, and Applications*, 20(10):1–19, 2024.
- [69] Aaron Van den Oord, Nal Kalchbrenner, Lasse Espeholt, Oriol Vinyals, Alex Graves, et al. Conditional image generation with pixelcnn decoders. *Advances in Neural Information Processing Systems*, 29, 2016.
- [70] Ashish Vaswani, Noam Shazeer, Niki Parmar, Jakob Uszkoreit, Llion Jones, Aidan N Gomez, Łukasz Kaiser, and Illia Polosukhin. Attention is all you need. *Advances in Neural Information Processing Systems*, 30:5998–6008, 2017.
- [71] Dezhao Wang, Wenhan Yang, Yueyu Hu, and Jiaying Liu. Neural data-dependent transform for learned image compression. In *Proceedings of the IEEE/CVF Conference on Computer Vision and Pattern Recognition*, 2022.
- [72] Huiyu Wang, Yukun Zhu, Bradley Green, Hartwig Adam, Alan Yuille, and Liang-Chieh Chen. Axial-deeplab: Stand-alone axial-attention for panoptic segmentation. In *Proceedings of the European Conference on Computer Vision*, pages 108–126. Springer, 2020.
- [73] Zhou Wang, Eero P Simoncelli, and Alan C Bovik. Multiscale structural similarity for image quality assessment. In *Asilomar Conference on Signals, Systems & Computers*, volume 2. IEEE, 2003.

- [74] Yaojun Wu, Xin Li, Zhizheng Zhang, Xin Jin, and Zhibo Chen. Learned block-based hybrid image compression. *IEEE Transactions on Circuits and Systems for Video Technology*, 32(6):3978–3990, 2022.
- [75] Yueqi Xie, Ka Leong Cheng, and Qifeng Chen. Enhanced invertible encoding for learned image compression. In *Proceedings of the 31st ACM International Conference on Multimedia*, pages 162–170, 2021.
- [76] Tongda Xu, Yan Wang, Dailan He, Chenjian Gao, Han Gao, Kunzan Liu, and Hongwei Qin. Multi-sample training for neural image compression. *Advances in Neural Information Processing Systems*, 35:1502–1515, 2022.
- [77] Qinhong Yang, Dongdong Chen, Zhentao Tan, Qiankun Liu, Qi Chu, Jianmin Bao, Lu Yuan, Gang Hua, and Nenghai Yu. Hq-50k: A large-scale, high-quality dataset for image restoration. *arXiv:2306.05390*, 2023.
- [78] Runyu Yang, Dong Liu, Siwei Ma, Feng Wu, and Wen Gao. Perceptual quality-oriented rate allocation via distillation from end-to-end image compression. *ACM Transactions on Multimedia Computing, Communications, and Applications*, 2024.
- [79] Runyu Yang, Dong Liu, Feng Wu, and Wen Gao. Learned image compression with efficient cross-platform entropy coding. *IEEE Journal on Emerging and Selected Topics in Circuits and Systems*, 2025.
- [80] Yibo Yang, Robert Bamler, and Stephan Mandt. Improving inference for neural image compression. *Advances in Neural Information Processing Systems*, 33:573–584, 2020.
- [81] Weihao Yu, Mi Luo, Pan Zhou, Chenyang Si, Yichen Zhou, Xinchao Wang, Jiashi Feng, and Shuicheng Yan. Metaformer is actually what you need for vision. In *Proceedings of the IEEE/CVF Conference on Computer Vision and Pattern Recognition*, pages 10819–10829, 2022.
- [82] Fanhu Zeng, Hao Tang, Yihua Shao, Siyu Chen, Ling Shao, and Yan Wang. Mambaic: State space models for high-performance learned image compression. In *Proceedings of the IEEE/CVF Conference on Computer Vision and Pattern Recognition*, pages 18041–18050, 2025.
- [83] Haotian Zhang, Li Li, and Dong Liu. Generalized gaussian model for learned image compression. *IEEE Transactions on Image Processing*, 2025.
- [84] Haotian Zhang, Feihong Mei, Junqi Liao, Li Li, Houqiang Li, and Dong Liu. Practical learned image compression with online encoder optimization. In *2024 Picture Coding Symposium (PCS)*, pages 1–5. IEEE, 2024.
- [85] Yulun Zhang, Kunpeng Li, Kai Li, Bineng Zhong, and Yun Fu. Residual non-local attention networks for image restoration. In *Proceedings of the International Conference on Learning Representations*, 2019.
- [86] Jing Zhao, Bin Li, Jiahao Li, Ruiqin Xiong, and Yan Lu. A universal optimization framework for learning-based image codec. *ACM Transactions on Multimedia Computing, Communications, and Applications*, 20(1):1–19, 2023.
- [87] Yinhao Zhu, Yang Yang, and Taco Cohen. Transformer-based transform coding. In *Proceedings of the International Conference on Learning Representations*, 2022.
- [88] Renjie Zou, Chunfeng Song, and Zhaoxiang Zhang. The devil is in the details: Window-based attention for image compression. In *Proceedings of the IEEE/CVF Conference on Computer Vision and Pattern Recognition*, 2022.